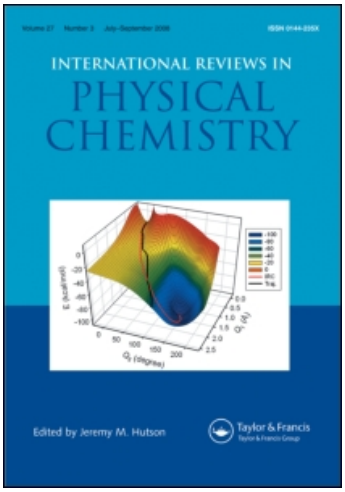

International Reviews in Physical Chemistry
Publication details, including instructions for authors and subscription information:
http://www.informaworld.com/smpp/title~content=t713724383

State-correlated DC slice imaging of formaldehyde photodissociation: roaming atoms and multichannel branching

Arthur G. Suits[a]; Steven D. Chambreau[a]; Sridhar A. Lahankar[a]
[a] Department of Chemistry, Wayne State University, Detroit, MI 48202

To cite this Article Suits, Arthur G. , Chambreau, Steven D. and Lahankar, Sridhar A.(2007) 'State-correlated DC slice imaging of formaldehyde photodissociation: roaming atoms and multichannel branching', International Reviews in Physical Chemistry, 26: 4, 585 — 607
To link to this Article: DOI: 10.1080/01442350701589908
URL: http://dx.doi.org/10.1080/01442350701589908

International Reviews in Physical Chemistry,
Vol. 26, No. 4, October–December 2007, 585–607

Taylor & Francis
Taylor & Francis Group

State-correlated DC slice imaging of formaldehyde photodissociation: roaming atoms and multichannel branching

ARTHUR G. SUITS*, STEVEN D. CHAMBREAU† and SRIDHAR A. LAHANKAR

Department of Chemistry, Wayne State University, Detroit, MI 48202

(*Received 7 July 2007; in final form 23 July 2007*)

High-resolution slice imaging methods allow for detection of single product quantum states with sufficient velocity resolution to infer the full *correlated* product state distribution of the undetected fragment. This is a level of detail not available in previous studies of formaldehyde photodissociation, and in this application it reveals startling new aspects of unimolecular decomposition. The CO rotational distributions from near ultraviolet dissociation of formaldehyde are bimodal, and the imaging experiments allow us to decompose these into two dynamically distinct components: the conventional molecular dissociation over a high exit barrier, and a novel 'roaming atom' reaction in which frustrated radical dissociation events lead to intramolecular H abstraction, bypassing the transition state entirely. In probing the dynamics of the conventional molecular dissociation over the barrier, we use the complete v_{H2}-j_{CO} correlation to model the exit channel dynamics in new detail. Furthermore, these state-correlated measurements provide insight into radical–radical reactions and the underlying dynamics and energy dependence of the roaming pathway.

Contents

*Corresponding author. Email: asuits@chem.wayne.edu
†Present address: Air Force Research Laboratory, Edwards AFB, CA.

International Reviews in Physical Chemistry
ISSN 0144–235X print/ISSN 1366–591X online
http://www.tandf.co.uk/journals
DOI: 10.1080/01442350701589908

1. Introduction

Photodissociation of formaldehyde ranks among the most thoroughly studied chemical reactions, and there are numerous reasons for this: it can be optically excited via rotationally-resolved metastable levels of the first excited singlet state (S_1) that subsequently lead to decomposition via a rich assortment of decay processes, so its photochemistry may be studied with single quantum state selectivity, and competition and interaction among these dissociation channels may be studied in great detail [1–21]. The dominant products following low energy excitation are two closed-shell diatomics, H_2 and CO, formed over a high barrier, while at somewhat higher energy a barrierless radical channel giving H + HCO opens and comes to dominate (see figure 1) [7, 16–22]. All of these products are amenable to sensitive detection via a variety of experimental techniques. Furthermore, with just sixteen electrons and six vibrational degrees of freedom, its relative simplicity allows for detailed characterization of the potential energy surfaces using high-level quantum chemistry methods and dynamical calculations [23–40]. Photoexcitation and dissociation of formaldehyde thus represents an ideal system with which to probe the details of many key issues in chemical physics. Indeed, these considerations have motivated decades of intense study summarized below. Despite this intense scrutiny over many years, formaldehyde still has a great deal to teach us, as these pages will show. With the advent of high-resolution slice imaging methods [41–43], single product quantum states may be detected with sufficient velocity resolution to infer the full *correlated* product state distribution of the undetected fragment. This is a level of detail not available in previous studies of formaldehyde, and in this application it reveals startling new aspects of unimolecular decomposition [44–47].

Figure 1 shows a schematic view of the relevant potential energy surfaces for formaldehyde excitation and dissociation in the near ultraviolet. The mechanism of these processes is summarized below:

$$H_2CO\ S_0(^1A_1) + h\nu \rightarrow H_2CO\ S_1(^1A_2) \quad (1)$$

$$H_2CO\ S_1(^1A_2) \rightarrow H_2CO\ S_0(^1A_1)\,(E, j)^* \quad (2)$$

$$H_2CO\ S_1(^1A_2) \rightarrow H_2CO\ T_1(^3A_2)\,(E, j)^* \quad (2')$$

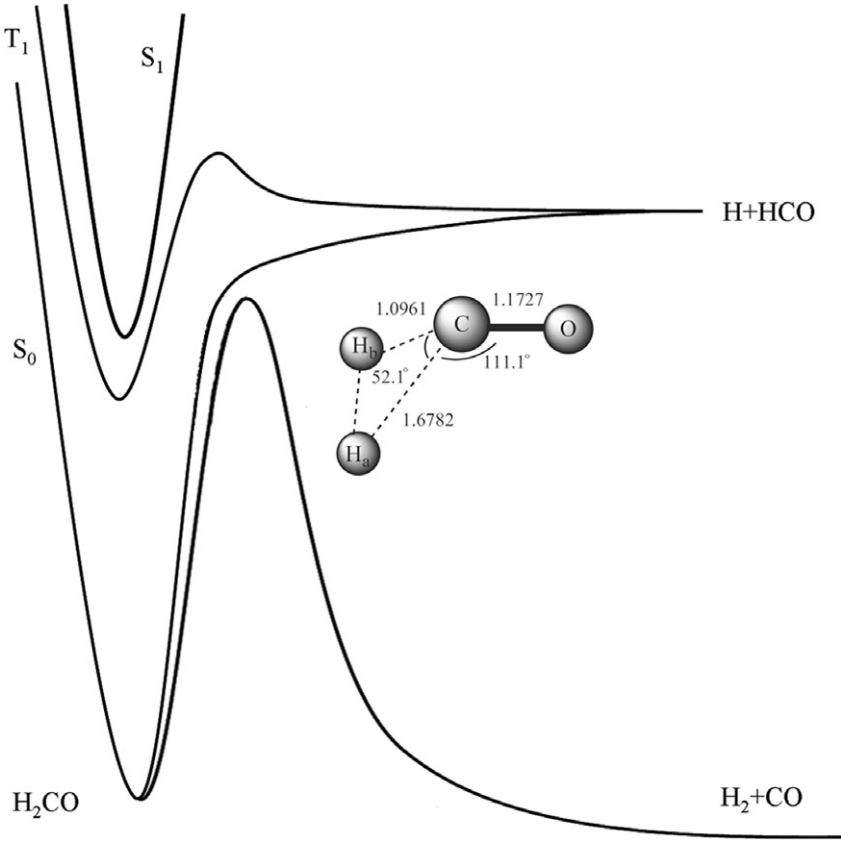

Figure 1. Schematic view of low-lying potential energy surfaces for H_2CO and transition state geometry for molecular dissociation from Reference 37.

$$H_2CO\ S_0(^1A_1)\,(E,j)^* \rightarrow H_2 + CO \tag{3}$$

$$H_2CO\ S_0(^1A_1)\,(E,j)^* \rightarrow H + HCO \tag{4}$$

$$H_2CO\ T_1(^3A_2)\,(E,j)^* \rightarrow H + HCO. \tag{4'}$$

Upon excitation to the first singlet excited electronic state S_1, (Reaction 1) formaldehyde rapidly undergoes internal conversion to high vibrational levels in the ground state (Reaction 2) or intersystem crossing to the triplet state (Reaction 2′). The barrier for the molecular dissociation channel (Reaction 3) inferred from the experiment is 27 720 cm^{-1} [15]. This channel has been extensively studied by Moore and coworkers [8–15]. They found that molecular elimination to H_2 and CO products proceeds by way of a skewed transition state in which both H atoms are on the same side of the CO bond axis (figure 1). This molecular dissociation leads to large

translational energy release, highly rotationally excited CO fragments, predominantly in the ground vibrational state, and low rotational and vibrational excitation in H_2. By fitting the CO rotational distribution with a modified impulsive model, Moore and coworkers found the resulting impact parameter for molecular elimination must be very large ($b \sim 1.0$ A) in order to produce such highly rotationally excited CO products [27]. The Moore group used coherent anti-Stokes Raman spectroscopy (CARS), Doppler spectroscopy, and vacuum ultraviolet laser-induced fluorescence (VUV-LIF) to measure the vibrational, translational, and rotational distributions of the H_2 and CO products and to determine the H_2 product vector correlations. They found that the CO angular momentum quantum number, j_{CO}, and the H_2 vibrational quantum number, v_{H2}, are highly inversely correlated, but that j_{CO} and j_{H2} are, at best, only weakly correlated. Note that these correlations are *average* correlations due to the separate nature of the experiments (correlations determined from separate experiments).

Moore and coworkers found that nuclear spin is largely conserved during the photodissociation process, so *para*- and *ortho*-H_2CO (even and odd K_a) yield *para*- and *ortho*-H_2 (even and odd j_{H2}), respectively [48]. The H_2 rotational distributions from dissociation of both *para*- and *ortho*-H_2CO were found to have Boltzmann-like distributions peaking at $j_{H2} = 3$–4. The *ortho* product for the $2^1 4^1$ excitation (mode 2 is the CO stretch and mode 4 is an out-of-plane bend, necessary to make these transitions weakly allowed) in S_1 has a spatial anisotropy parameter, β, near zero, but non-negligible anisotropy was seen on certain transitions in the *para* product; However, overall, β is small. Moore found the isotopologues HDCO and D_2CO exhibit increased rotational excitation of CO, as would be expected in the impulsive picture due to the increase in the reduced mass. Higher excitation in the H_2CO parent rotation in S_1 leads to broadening of the CO rotational distributions, but does not significantly shift the peak in the j_{CO} distribution. In an important paper in 1993, van Zee *et al*. reported bimodal CO rotational distributions above the threshold for the radical channel, $H_2CO \rightarrow H + HCO$ and hypothesized these were the result either of dissociation from two distinct geometries in the TS, or possibly to interactions with the radical channel [15]. This intriguing observation motivated our entry into the study of formaldehyde, and it will be the focus of Section 4 below.

At higher energies ($> 30{,}328.5\,cm^{-1}$), formaldehyde photodissociation also yields H and HCO radicals (Reaction 4). Kable and coworkers have investigated this channel in detail, [16, 18] and they reported the product state distribution of HCO [18]. For the $H + HCO$ channel on the S_0 surface, Terentis and Kable [16] examined HCO product state distributions near the threshold of the radical channel. They also found that when conservation of energy and angular momentum are enforced, phase space theory reproduces the experimental product state distribution. Kable [20] and coworkers extended the energy range even further, above the T_1 radical threshold, and Kable and Bowman [21] have recently published experimental and quasiclassical trajectory calculation (QCT) results for contributions from the T_1 surface to the $H + HCO$ product distributions. The reverse barrier on the T_1 surface is $1920\,cm^{-1}$ [49]. Wittig and coworkers reported the internal state distribution of product HCO by detecting the H atom fragment using the hydrogen-atom Rydberg time-of-flight technique (HRTOF) and reported that HCO has maximal rotational excitation in $K_a = 6$, $v = 0$ [17]. They suggested that radical dissociation on the singlet ground state is dominant at

energies above the H + HCO threshold yet below the barrier of the triplet surface (32,248.5 cm^{-1}), while above the triplet barrier, dissociation on the triplet surface will likely dominate [19–21].

Photodissociation dynamics studies have long focused on measuring scalar quantities such as product state distributions or translational energy release, or vector quantities such as spatial anisotropy or angular momentum polarization [50]. Many studies have gone beyond this to examine correlations among these observables, such as speed-dependent spatial anisotropy (a vector–scalar correlation), or angle-dependent angular momentum polarization, (a vector–vector correlation, often simply referred to as 'vector correlation') [51–59]. These studies can probe the dynamics in the molecular frame, or reveal features of the dissociative potential energy surface directly, and offer deep insight into the photodissociation event. In general, these approaches all refer to correlations among the properties of a single detected species. However, for many systems, deeper insight may be achieved by measuring the correlations between observables for distinct photoproducts [60, 61]. Slice imaging measurements now readily provide extraordinary velocity resolution for quantum state-selected products [42, 62, 63]; this then allows one to obtain the complete product state distribution for all co-products of a single detected quantum state. A series of such measurements thus allows one to construct the complete *joint product state distribution*, affording a new level of insight into the reaction dynamics of polyatomic molecules, as we will see demonstrated for the case of formaldehyde in what follows.

These state-correlated measurements are not unprecedented. The earliest such study, by Ticktin and Huber [60], was a measure of Doppler profiles for state-selected NO molecules following dissociation of methyl nitrite, from which the correlated CH_3O internal state distribution was inferred. However, no significant correlations were found in that system. Soon after, Gericke *et al.* [61] reported analogous measurements for OH from H_2O_2 dissociation at 193nm, and Broaurd [64] reported state correlations for vibrationally mediated dissociation of H_2O_2; In this system, a strong positive correlation of the rotational distributions of the two OH products was found and ascribed to torsional motion in the dissociation event. A series of such studies for the case of ketene photodissociation, beginning with work from the Wodtke group using CO metastable time of flight detection [65, 66], demonstrated the power of the approach to probe details of unimolecular dissociation dynamics [67, 68]. These measurements have been reported in other photochemical systems as well, and recently Liu and coworkers have used slice imaging to carry this strategy into the domain of reactive scattering [43, 69–71].

In this review, we highlight the use of detailed state-correlated imaging measurements to reveal new aspects of reaction dynamics, with unimolecular dissociation of formaldehyde as our focus. The structure of the paper is as follows: we begin with an overview of the DC slice imaging approach and its application to H_2CO dissociation. This method allows direct detection of the velocity distribution of the central section of the recoiling product sphere, without need for deconvolution or fitting. We then show use of this method to obtain the complete joint probability distribution for the conventional molecular channel in H_2CO dissociation, and discuss implications of these measurements. We then turn to a presentation of a new 'roaming atom' reaction mechanism identified in these studies. We document the evidence for this phenomenon

and use the state correlated measurements to probe the detailed dynamics of what is, in essence, an intramolecular abstraction reaction. We then turn to an examination of the energy dependence of this process and the multichannel branching in this system. Finally, we offer some conclusions and perspectives for the future of these studies.

2. Experimental

The DC slice imaging apparatus used in these studies has been described in detail, previously [42, 62]. DC slice imaging [42] is a high-resolution adaptation of velocity map imaging [72] and its predecessor, ion imaging [73]. In these experiments, a molecular beam of formaldehyde seeded in argon is expanded from a piezoelectric pulsed valve, is skimmed, then enters the interaction/detection chamber on the axis of a time of flight mass spectrometer with a position sensitive microchannelplate (MCP) detector viewed by a video camera. The jet-cooled formaldehyde is excited via discrete levels in S_1 using a tunable UV laser from 300–330 nm. Excited molecules undergo internal conversion to the ground state and dissociate some nanoseconds later. The CO product is then ionized quantum state selectively using $2+1$ resonant multiphoton ionization on the *B-X* transition. The probe laser was typically scanned across the Doppler profile of the transition to ensure uniform detection efficiency regardless of recoil speed or direction. CO^+ ions were accelerated under DC slice imaging conditions onto the MCP/phosphor screen detector. The DC slice imaging approach allows for the central section of the photofragment ion cloud to be recorded exclusively, by stretching the ion cloud along the time of flight direction so that a narrow high voltage gate pulse applied to the detector selects only that portion of the distribution. Velocity and angular distributions for a photodissociation event are thus obtained without the need for reconstruction methods otherwise necessary to obtain the three dimensional distribution from its two dimensional projection. The recently developed megapixel (IMACQ) software developed in our group affords sub-pixel resolution using a standard (512×480 pixel) CCD camera [62]. The finite slicing algorithm of Hall and coworkers further increases the resolution of the DC slicing imaging approach by correcting for different slice widths for slow versus fast photofragments [68].

Photofragment excitation (PHOFEX) spectra were obtained by fixing the probe laser on the centre of a particular CO probe transition with the detector gate set to record all CO^+ signal (unsliced condition). The photolysis laser was then scanned while recording total signal from the phosphor screen using a photomultiplier tube. A typical PHOFEX spectrum for CO^+ ($v=0, j_{CO}=45$) obtained on the $2^1 4^3$ band is shown in figure 2, along with a simulation from the ASYROT program [74, 75]. The spectrum shows discrete rotational levels in S_1 and is fitted to a rotational temperature of $\sim$5 K.

The images included here were typically averaged over 400 000 laser shots. The translational energy distributions were obtained by integrating over the angular distributions and applying the appropriate Jacobian for conversion from velocity space to energy space. The velocity resolution in these studies is typically on the order of 20 m/s, with the limit set by CO^+ recoil from the electron owing to excess energy in the REMPI process [62].

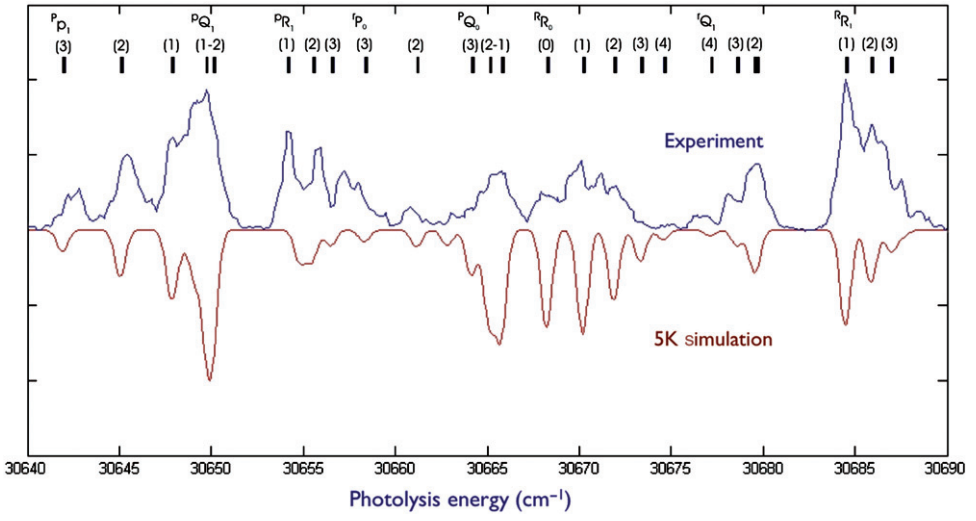

Figure 2. PHOFEX spectrum and simulation for jet-cooled formaldehyde recorded on $j_{CO} = 45$ following dissociation via the $2^1 4^3$ band.

3. Dynamics of the conventional molecular channel

This review describes a series of investigations exploring the detailed correlations between the rotational angular momentum of the CO fragment and the corresponding vibrational quantum states of the H_2 cofragment following photodissociation of H_2CO. In addition, we examine the correlation of the *rotational* distributions of the H_2 photofragment with those of the CO, although the correlation between j_{CO} and j_{H2} is much less pronounced than the correlation between $v_{H_2}$and j_{CO}. In this first section, we focus on the conventional molecular dissociation over the barrier, extending the treatment outlined by Moore and coworkers [9]. A simple dynamical model relying on density functional theory (DFT) calculations of the displacement vectors along the reaction coordinate is presented to give insight into the strongly correlated $v_{H_2}$and j_{CO} distributions following photodissociation of H_2CO.

3.1 *Molecular* vs. *roaming dissociation*

As first reported by van Zee and coworkers, photodissociation of formaldehyde above the threshold for the radical channel results in bimodal CO product rotational distributions [15]. Our DC sliced images and the corresponding translational energy distributions of these state-selected CO products, shown in figure 3, also show two characteristic translational energy distributions that reflect coincident formation of two distinct populations of H_2 internal states. The larger translational energy release products, associated with H_2 in vibrational levels from 0 to 4, are associated with the high CO rotational states and are similar to the distribution seen for photodissocation below the radical threshold (compare figure 3A and B). This is the conventional

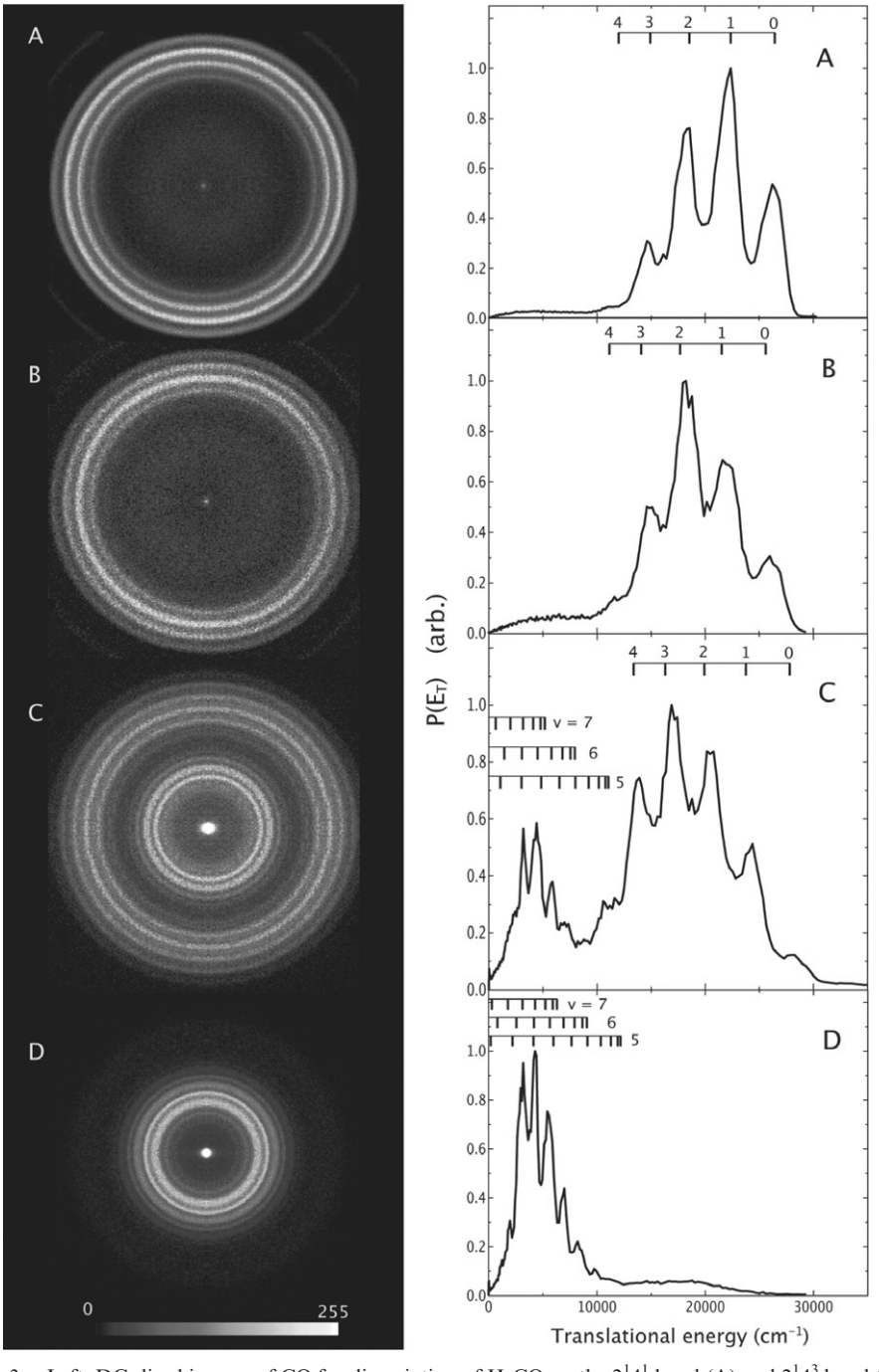

Figure 3. Left: DC sliced images of CO for dissociation of H_2CO on the $2^1 4^1$ band (A) and $2^1 4^3$ band (B-D) for $j_{CO} = 40$ (A,B); $j_{CO} = 28$ (C) and $j_{CO} = 15$ (D). Right: translational energy distributions obtained from the corresponding images at left. Markers indicate correlated H_2 vibrational levels for $j_{H2} = 5$ (for $v = 0$–4) or rovibrational levels (for $v = 5$–7). Reproduced from J. Phys. Chem. A, **109**(39) 8666, Copyright 2005 American Chemical Society.

molecular channel. Low rotational levels of CO are formed in coincidence with very high vibrational levels of H_2, typically $v = 6$–8 (see figure 3D). Intermediate rotational levels clearly show both populations as a bimodal distribution (figure 3C). This channel producing low rotational levels of CO with high vibrational excitation in H_2 is termed the 'roaming atom' pathway, and is discussed in detail in section 5. In this section, we focus on the dynamics underlying the conventional molecular channel.

3.2 *Correlated state analysis of the conventional molecular channel*

Numerous sliced ion images for spectroscopically-selected CO rotational levels were obtained and analysed to yield the corresponding translational energy distributions (see figures 1–4 of ref. [45]). The structure of the translational energy distributions reflects the internal energy of the H_2 cofragment. These translational energy distributions were fitted with Gaussian functions to determine the peak area. To obtain the global correlated state distributions, the image intensities (total peak areas) were scaled relative to each other to fit the CO rotational distributions of van Zee *et al.* [15] The resulting correlated v_{H_2}, j_{CO} plot for the $2^1 4^3$ transition from $v_{H_2} = 5$ can be seen in figure 4. From figure 4, slices along a given j_{CO} embody the translational energy distributions obtained directly from the images. If slices orthogonal to the j_{CO} direction (along each v_{H_2} are taken instead, the result shown in figure 5 is obtained. Figure 5 shows the correlation between v_{H_2} and j_{CO} as v_{H_2} increases from 0 to 5. Similar analyses were performed for other photolysis energies. We should emphasize that figure 5 shows CO rotational distributions for particular H_2 vibrational states, even though H_2 was

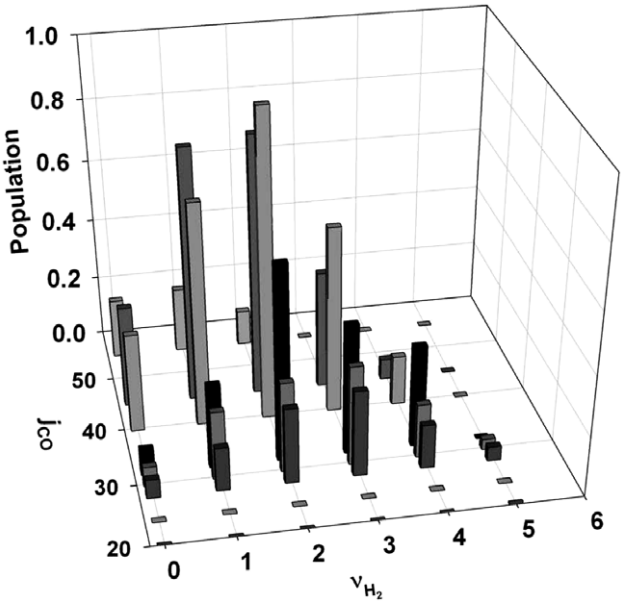

Figure 4. Correlated state plot, j_{CO} versus v_{H_2} for H_2CO photolysis at the $2^1 4^3$ transition. CO rotational distributions as a function of v_{H_2} for H_2CO photolysis via the $2^1 4^3$ band. Reproduced from J. Chem. Phys. **125** 044302, Copyright 2006, American Institute of Physics.

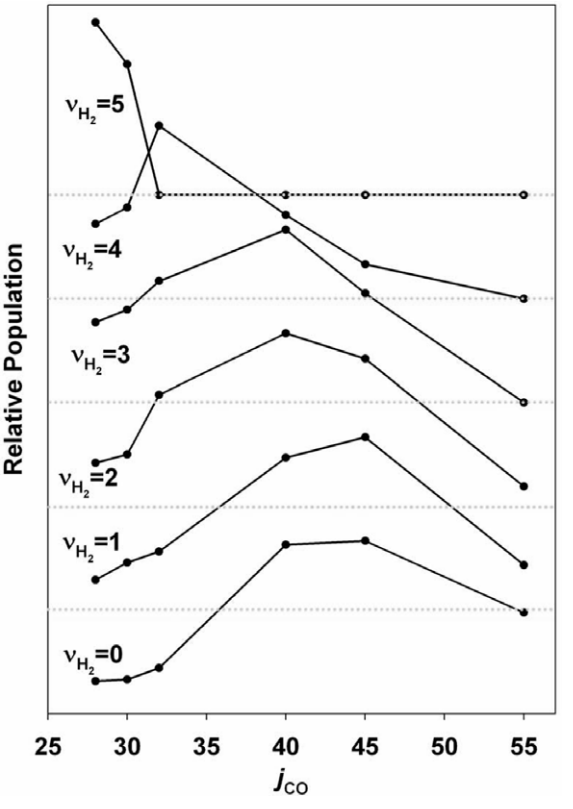

Figure 5. CO rotational distributions as a function of v_{H_2} for H_2CO photolysis at 2^14^3 (see text). Reproduced from J. Chem. Phys. **125** 044302, Copyright 2006, American Institute of Physics.

never detected in these experiments. These correlations are key to understanding the dynamics, as shown in the next subsection.

The translational energy distributions could also be fitted to reveal the H_2 rotational distributions. In order to test the validity of this approach, the H_2 rotational distributions from the fit for the most populated CO levels were compared to the experimental H_2 rotational distributions of Debarre [12] at the same excitation energy (29,496 cm^{-1}, 2^14^1) obtained using Coherent Anti-Stokes Raman Spectroscopy (CARS). The agreement with the CARS data was very good. All the translational energy distributions were then analysed to reveal the j_{H2}-j_{CO} correlations (see figure 10 of ref. [45]). However, little correlation was seen for rotation alone. This has been rationalized by Schinke, [36] who argued that the magnitude of the potential terms that couple rotations in CO and H_2 simultaneously are very small.

We return to consider the v_{H2}-specific CO rotational distributions in figure 5 after photodissociation on the 2^14^3 band. These distributions match well with the results from the modified impulsive model described below, and the distribution widths are also comparable [9]. The shift to lower CO peak values with increasing H_2 vibrational excitation accounts for the slight asymmetry of the total CO rotational distribution

above $j_{CO} \sim 25$ seen by van Zee [15]. A similar shift is seen for the $2^2 4^1$ transition (see figure 9 of reference 45), although the peak in j_{CO} at high H_2 vibrational levels does not drop off as dramatically as for $2^1 4^3$. This can be explained by the higher photoexcitation energy shifting the CO rotational distributions to higher j_{CO} peak values, and was also observed by van Zee [15].

The strong correlation between the rotational states of CO and the vibrational states of H_2 can be explained by the dynamical influence of the highly repulsive exit channel on the H_2CO potential energy surface. In short, for each H_2 vibrational level, there is a distinct available energy, and a highly constrained dissociation geometry that determines the exit impact parameter. These two things together then determine the CO rotational distributions. Bamford suggested that looking at the change in directions of the reaction coordinate vectors as the molecule moves from the transition state to products would give insight into the dynamic character of this system [8]. The following section describes how this simple dynamical model was formulated, and how the impact parameters corresponding to each H_2 vibration were determined. While this modified impulse model reproduces the H_2 and CO rotational distributions well, it cannot account for subtle details in the shape of the potential surface or quantum effects in the transition state [9].

3.3 *Dynamical model for molecular elimination*

To model the dissociation dynamics, the reaction coordinate was calculated using a Gaussian 03 [76] internal reaction coordinate (IRC) calculation at the B3LYP 6-31+G(d,p) level of theory [45]. At points along the IRC corresponding to the classical outer turning points of H_2 vibration for $\nu_{H_2} = 0$–5 (figure 6), vibrational frequencies were calculated and the frequency corresponding to the reaction coordinate was identified. The molecular displacement vectors for the reaction coordinate were then determined, and the corresponding impact parameter evaluated for an impulse occurring at that geometry, as seen in figure 6 for $\nu_{H_2} = 0$–5. Using the modified impulsive model [8] the rotational energy of the CO product could then be readily obtained from the impact parameter. As the vibrational level of the H_2 product decreases over the barrier, E_{avl} increases accordingly. Calculated impact parameters and corresponding CO rotational levels are given for $\nu_{H_2} = 0$–5 in Table 4 of Reference 45. These results are in reasonable agreement with those of Butenhoff, Carleton, and Moore [9] at $2^1 4^1$, and clearly account for the large CO rotational excitation in photodissociation of H_2CO, peaking around $j_{CO} = 40$ for the transitions investigated. We should note, however, that the change in these correlated distributions with excitation energy is much smaller in the model than seen experimentally (compare figures 5 and 6). This suggests more complex exit channel effects and the importance of trajectories that deviate from the minimum energy path.

4. The roaming atom pathway

Dissociation of energized molecules to closed-shell products generally results in large translational energy release in the fragments owing to Pauli repulsion of the electron

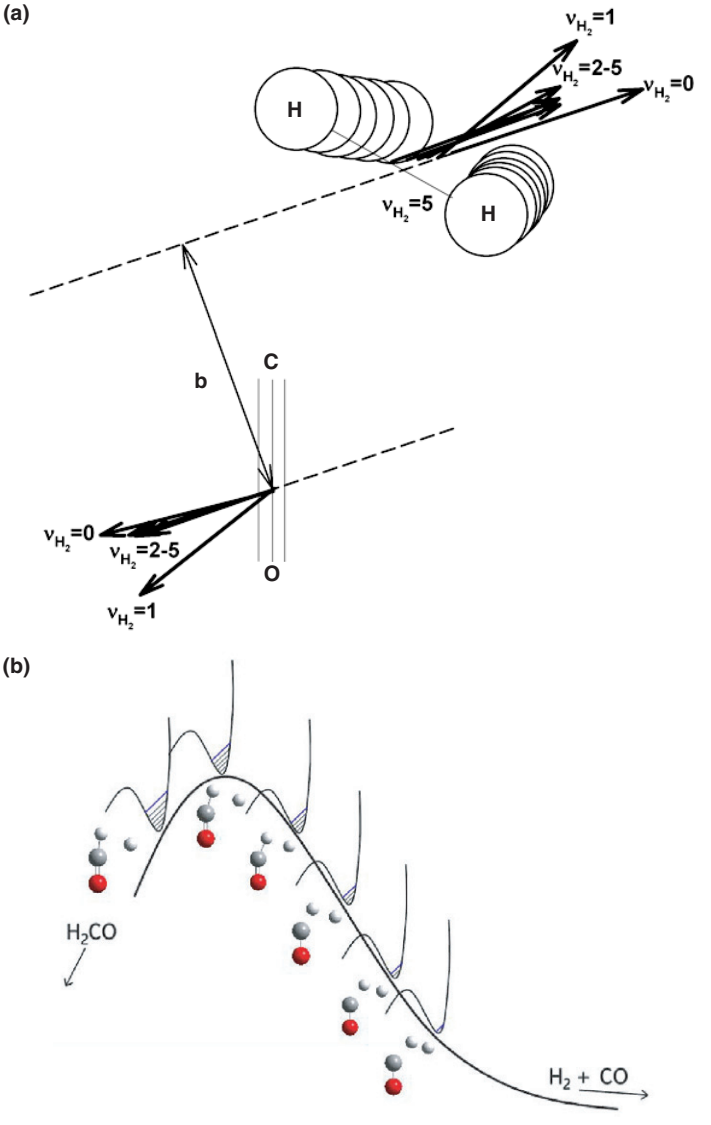

Figure 6. Dynamical model for the molecular elimination of H_2CO: (a) The top hydrogen atoms correspond to the geometry for $\nu_{H_2} = 5$, and subsequent circles are for $\nu_{H_2} = 4 \rightarrow 0$. (b) Progression of H_2CO on the internal reaction coordinate for molecular elimination. Each geometry corresponds to the r_{H-H} classical turning point for $\nu_{H_2} = 5$ to 0 (left to right). See text for more details. Reproduced from J. Chem. Phys. **125** 044302, Copyright 2006, American Institute of Physics.

clouds of the newly-formed molecules. This repulsive interaction gives rise to a significant barrier to the reaction, and the potential energy of this exit barrier is efficiently converted to relative kinetic energy of the fragments as the molecule dissociates. This is precisely what is seen for the conventional molecular channel in formaldehyde dissociation summarized in the preceding section.

Furthermore, the structure and vibrational frequencies of the molecule at the top of the barrier, the transition state, are of profound importance in determining the rate of reaction or dissociation and the concept of the transition state is thus central to the remarkably successful statistical theories of chemical reactions. These theories began with Eyring's work [77, 78] in the 1930s and have evolved to Rice–Rampsberger–Kassel–Marcus (RRKM) theory and related approaches in the present day [79]. All of these theories represent the rate of reaction as proportional to the ratio of the number of accessible quantum states of the transition state to the density of quantum states of the reactants. The properties of the transition state are thus key to understanding the basis of chemical reaction rates. However, recent studies have begun to appear that challenge this 'central dogma' of transition state theory and point to the need to consider alternative reaction mechanisms. One such important example arose in investigations of the reaction $O(^3P) + CH_3$ studied experimentally by Leone and coworkers, and theoretically by Klippenstein, Harding and coworkers [80]. Prompt CO was clearly seen in FTIR studies and ascribed to $O + CH_3 \rightarrow CH_3O^* \rightarrow H_2 + HCO^* \rightarrow H_2 + H + CO$. However, no transition state could be found to account for this. The mechanism was finally identified in direct-dynamics trajectory calculations, and termed an 'over-the-ridge' reaction in which a departing H atom abstracts another H atom in the course of dissociation. In theoretical calculations on other systems, such as high energy $O(^3P)$ + ethane reaction, similar non-TS dynamics have been seen [81]. We should note that a related mechanism was proposed by Jackson and coworkers [82] to account for formation of NO + CO in the reaction of CN with O_2, but this has not yet been confirmed. We will see all of this behaviour is closely related to the roaming mechanism in formaldehyde, in which it is clearly demonstrated both experimentally and theoretically.

As sketched in section 3.1, one subtle feature of the molecular channel measurements did not fit well with the impulsive view of the molecular dissociation dynamics: van Zee *et al.* noted [15] that when formaldehyde was excited above the threshold for the H + HCO dissociation channel, the CO rotational distributions exhibited an unusual shoulder to lower rotational levels, while below the radical threshold, essentially no CO was produced in rotational levels below $j_{CO} = 20$ or so. Van Zee and coworkers proposed two possible explanations for this: one explanation was that at higher energies the transition state region may sample additional geometries that lead to reduced exit impact parameters hence lower rotational excitation in the CO. The second possibility was that the low-J CO was somehow directly related to the opening of the radical dissociation channel and a distinct new pathway to formation of molecular products. This was the explanation they favoured, and we will see, one that clearly points to the essential dynamics.

4.1 *Roaming atom H abstraction dynamics*

In figure 5 we showed the correlated state plot indicating the joint probabilities for forming low vibrational levels of H_2 with high rotational levels of CO. In figure 7A, we present an alternative view of this data for the $2^1 4^3$ transition, expanded to

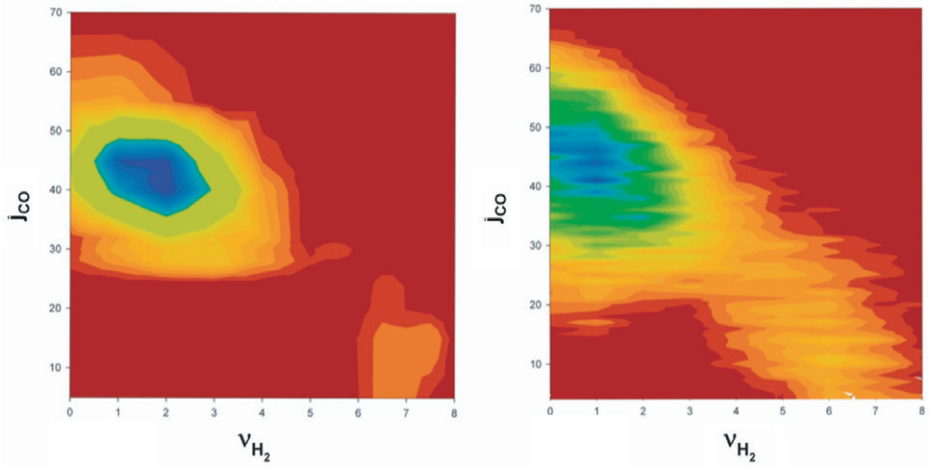

Figure 7. Product state correlation plot at $2^1 4^3$ from experiment (a) and from QCT calculations (b).

include very high vibrational levels of H_2 and low rotational levels of CO. This is shown in comparison with the identical data obtained from QCT calculations from the Bowman group (figure 7B). Both plots show two distinct isolated regions, clearly indicating dynamically distinct processes. The dominant region in the upper left corresponds to simultaneous formation of rotationally hot CO and vibrationally 'cool' H_2, and is well-explained by the impulsive picture of the preceding section. The other region, in the lower right, is associated with very highly vibrationally excited H_2, up to $v = 8$, formed with rotationally cold CO. Our task now is to account for the formation of this region of the joint state plots.

We first anticipate what to expect relying solely on our intuition. If, as van Zee *et al.* suspected, this new channel arises somehow from the radical dissociation, then an intramolecular abstraction reaction is the likely mechanism. That this is true is strongly supported by van Zee's observation that this low-J shoulder in CO first appears at excitation energies essentially coincident with the opening of the radical channel. What distributions, then, might we expect for an H + HCO reaction at essentially zero kinetic energy? This is a highly exoergic, barrierless radical–radical reaction. In the Polanyi picture this is the extreme of the 'early barrier' case, in which very high vibrational excitation is expected in the new H–H bond, and little translational energy release, hence little rotational excitation, is expected in the CO. This is precisely what is seen in the lower right of figure 7. Our intuition, then, suggests that this dynamically distinct region in figure 7 is consistent with an intramolecular H abstraction reaction in which a departing H atom returns from a frustrated radical dissociation event to react to form molecular products.

Fortunately, we do not need to rely on our intuition alone. The theoretical calculations from the Bowman group allow for a detailed quantitative understanding of this process. The theoretical calculations agree remarkably well with the experimental results, showing, for this distinct region, H_2 vibration up to $v = 8$ correlated to CO in rotational levels $j_{CO} = 10$–15. A further advantage of the

Figure 8. A sample roaming trajectory yielding H_2 $v=6$ and $j_{CO}=5$. Only H atoms are shown. H atom speeds are encoded in trajectory colour and forces (direction and magnitude) are shown at 1 fs intervals in abstraction region.

calculations is that we may closely examine individual trajectories for deeper insight into the dynamics. One such trajectory, associated with formation of H_2 in $v=6$ and CO in $j_{CO}=7$ is shown plotted in figure 8. This figure was developed by F. Suits at IBM from trajectory calculations by Zhang and Bowman. [46] Only the H atom motions during the course of dissociation are shown, beginning at the left, with the C and O atoms omitted. One H atom is seen in the upper part of the figure undergoing large amplitude motion while the other undergoes complex small amplitude motions. At one point, the upper H atom nearly undergoes complete dissociation, roaming broadly in a flat, remote region of the potential. At the same time, the remaining H atom is bound to the CO, and this HCO molecule can be seen to undergo out-of-plane rotation (the two loops in figure 8). The roaming H atom then returns to the HCO, and in the region of the abstraction reaction, force vectors are also shown for the two H atoms. Reaction occurs (the large, outward pointing force vectors indicate the inner turning points of the newly formed H_2 vibration) and the H_2 molecule is emitted to the right. This trajectory forms molecular products H_2 and CO, but goes nowhere near the configuration of the TS shown in figure 1, and gives rise to an entirely different product state distribution.

As suggested above, this roaming atom pathway actually affords the opportunity for a deep investigation of H abstraction in a radical–radical reaction, and we just sketch this here. The experiments allowed for the direct determination of the H_2 rotational distributions for the roaming channel [46], and this was found to peak at $j_{H2}=7$–9, considerably higher than for the case of the dissociation via the conventional transition state despite the absence of the repulsive exit barrier for the roaming case. Scans of the potential surface showed little tendency to constrain the reaction to the plane, but a clear tendency to emit the bound atom along the HCO equilibrium bond angle regardless of the approach direction of the roaming hydrogen atom.

This emission can be viewed in a 'direct interaction – product repulsion' picture to account for the non-negligible translational energy release seen as well.

4.2 *Implications of roaming pathways*

We now turn to a discussion of the roaming dynamics and their broader implications. There are a number of questions that arise immediately: how general is this phenomenon? Something similar was seen in H_3CO, as well as H_2CO, so is it confined to H roaming and H abstraction reactions? Is it a threshold phenomenon, and if not, what is its energy dependence? And how does this fit into a larger picture of reaction dynamics and what are the implications of this for transition state theory?

We take the easier questions first. Houston and Kable have recently seen evidence in CO Doppler profiles and vector correlations for an analogous process in acetaldehyde dissociation [83] Further support for this has come from theoretical calculations by Bowman *et al*., and more recent imaging experiments from Banares and coworkers [84]. In this system, energetics suggest it must be the methyl group that is 'roaming'. This clearly points the way to future studies.

The question of whether it is a threshold phenomenon can also be addressed immediately. That roaming in H_2CO persists well above the threshold for the radical dissociation is suggested in the original work of van Zee *et al*., considered in light of the results discussed in the preceding paragraphs, and it is confirmed both in QCT calculations from Bowman [38], and in our own imaging experiments [47]. This detailed energy dependence is the focus of section 5.

The implications of roaming for transition state theory (TST) are less clear. One might argue that at this energy, well above the molecular channel barrier, the transition state dividing surface extends over broad regions of configuration space, and roaming just represents another example of reaction far from the minimum energy path (MEP). This view is somewhat reminiscent of the first suggestion of van Zee *et al*, i.e., that anharmonicity at the TS leads to dissociation from distinct geometries, giving rise to distinct rotational distributions. However, roaming appears qualitatively distinct from the normal TS pathway and to try to encompass it within conventional TST seems use of the wrong 'basis set' to describe the problem. We already have a sense that roaming is much more closely related to the radical dissociation than the conventional molecular dissociation, and we will consider this further in the next section. However, it is not yet clear how to join the two to get a succinct prediction of the kinetics of molecular product formation that includes roaming. At any rate, at present there is no universal way to patch TST to account for roaming reactions.

Zare and Hase [85] have pointed out that the production of highly excited products is a signature of dynamics that stray from the MEP, and this is an instructive perspective. They have noted that roaming dynamics are, in a sense, an extreme example of this. One should not lose sight of the fundamentally distinct character of roaming, however. Moreover, we note that a portion of the roaming pathway actually corresponds closely to the MEP for the for the $H + HCO$ abstraction reaction, and these highly excited products are simply characteristic of this reaction. Ongoing discussion of these issues clearly leads to an appreciation of the richness and complexity of unimolecular reaction dynamics, and deeper insight as well.

5. Energy dependence of roaming and multichannel branching

5.1 *PHOFEX spectra*

We noted in the previous section that roaming is not a threshold phenomenon, and we now examine its detailed energy dependence in H_2CO dissociation. Figure 9 shows a survey photofragment excitation (PHOFEX) scan with detection of two different rotational levels of CO: $j_{CO} = 45$ and 15. We have shown the former corresponds exclusively to the conventional molecular channel, while the latter corresponds exclusively to the roaming pathway (see figure 7). It is clear from this figure that the roaming contribution grows in importance relative to the conventional molecular channel with increasing energy. Although these PHOFEX spectra are strongly suggestive, they are not quantitative. To convert these to actual branching fractions, we have analysed many images obtained for a range of CO rotational levels on the $2^1 4^3$ transition to identify the roaming fraction in each (see figure 11 of ref. [46]). This then allowed us to determine the overall branching to roaming on this transition, and we find a value of 18%. Using this value, we then normalized the PHOFEX branching for $j_{CO} = 15$ and 45 to give the overall energy dependent branching. This is shown in figure 10, in which we see the fraction of molecular products formed via the roaming mechanism rises until it is nearly equal to the fraction formed via the conventional dissociation pathway about 1500 cm^{-1} above the radical threshold.

5.2 *Multichannel branching*

An important question remaining now is the branching between the molecular products, which we have decomposed into roaming and conventional pathways, and the radical products. Unfortunately, it is not easy to get at this experimentally. There are two strategies we can use for this relying on theoretical input. One uses microcanonical

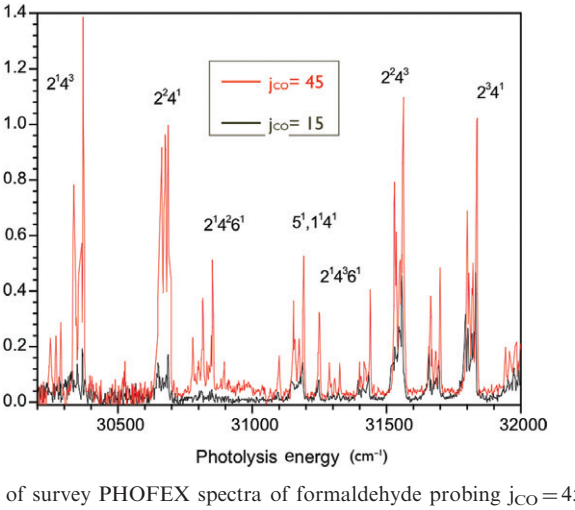

Figure 9. Comparison of survey PHOFEX spectra of formaldehyde probing $j_{CO} = 45$ (light) and $j_{CO} = 15$ (dark). Reproduced from J. Chem. Phys. **126** 044314, Copyright 2007, American Institute of Physics.

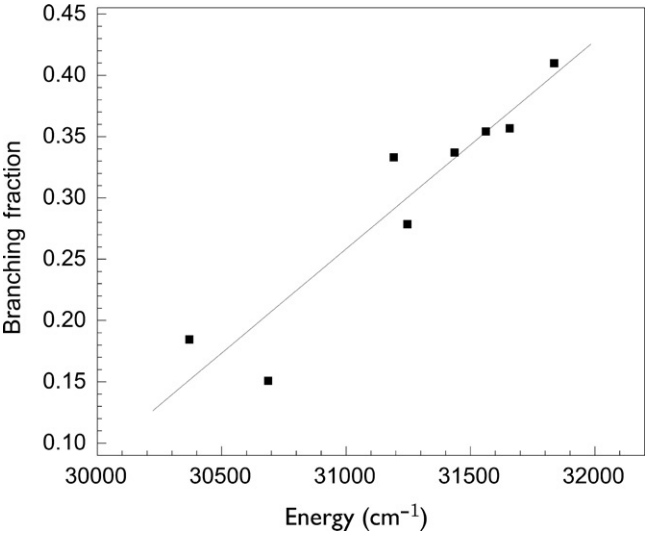

Figure 10. Energy dependent fraction of molecular products via roaming pathway.

rate calculations performed by Troe, who has considered the multichannel branching in H_2CO in a series of papers recently [86–88]. The other strategy relies on branching determined using the QCT calculations.

Troe independently estimated the rates of the conventional molecular channel using a Rice Ramsperger Kassel and Marcus (RRKM) model and for the radical channel using the Statistical Adiabatic Channel Model (SACM) [86] at a series of energies. Troe's calculated rates show that branching to radical products dominates by at least an order of magnitude as soon as that channel is open owing to the tight transition state for the molecular channel and the large A-factor for the radical dissociation. As a result, in the multichannel analysis, he assumed that essentially all molecular products formed above the radical threshold must arise from roaming. Our results clearly show that this is not the case. We thus turn to an alternative approach to estimate the multichannel branching using the results of the QCT calculations reported by Bowman and coworkers [38]. Their energy-dependent branching between molecular and radical products shows a much more gradual onset, reaching a maximum yield of 75% for the radical channel at 1700 cm^{-1} above threshold. We can estimate experimental values for the overall branching fractions by scaling our roaming *vs.* molecular branching shown in figure 10 to the QCT calculations. Figure 11 shows the result of this analysis. As the radical channel opens, it grows in and comes to dominate over a range of 1500–2000 cm^{-1}. At the same time, branching to the conventional molecular channel drops rapidly. Branching to roaming, however is nearly flat, just slightly decreasing with energy above threshold. This observation leads us to a deeper examination of the dynamics of the roaming process itself.

5.3 *Energy dependent dynamics of roaming*

If we consider the dynamics underlying the roaming trajectory shown in figure 8, and again rely on our intuition for guidance, we can readily understand the multichannel

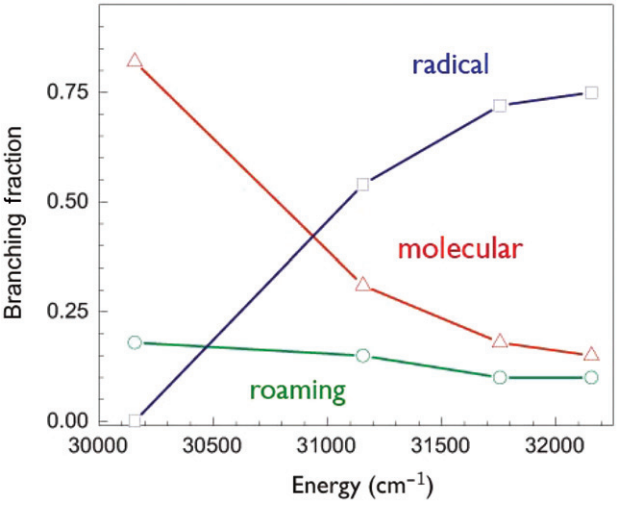

Figure 11. Energy dependent multichannel branching.

branching shown in figure 11. We have seen that roaming arises from the radical dissociation. However, these are radical dissociation trajectories lacking sufficient energy in the reaction coordinate for complete dissociation. For barrierless unimolecular dissociation of a polyatomic molecule, there are generally many such events. As the excess energy grows, this fraction may drop relative to those that do have sufficient energy to dissociate, but it will be a gradual decrease, while at the same time the radical dissociation, from which roaming derives, will tend to grow relative to molecular dissociation via a tight TS. Our intuition thus leads us directly to the branching shown in figure 11. The key point remaining is to determine precisely the window for which roaming trajectories are possible. Fortunately, several transitions span the radical threshold in H_2CO, so we can use PHOFEX on low and high rotational levels in CO to bracket this onset. Such a spectrum is shown in figure 12, using $j_{CO} = 15$ as the roaming marker and $j_{CO} = 45$ for the conventional molecular channel as before. The radical threshold is also marked in the figure, and we see the roaming persists 90 cm^{-1} below the radical onset (the $2^1 6^1$ bands appear both at $j_{CO} = 15$ and 45), but it is gone at 150 cm^{-1} below (the 4^5 band is clear in $j_{CO} = 45$ but missing in the $j_{CO} = 45$ spectrum). Our roaming window, in the case of formaldehyde, thus extends at least to $\sim$100 cm^{-1} below the radical dissociation threshold. Furthermore, as long as there are product states of HCO no farther apart than this as the energy is increased, we will have a 'roaming continuum' as the excitation energy increases. However, the fluctuation of the density of such states with energy may well influence the detailed branching and give some the appearance of mode specificity. Finally, we note that this window is strictly determined only for H_2CO, and details of the potential surface will clearly affect it for other systems.

6. Conclusions and outlook

We have shown that fully state-correlated imaging studies can deliver deep new insights into fundamental chemical processes, and formaldehyde clearly represents

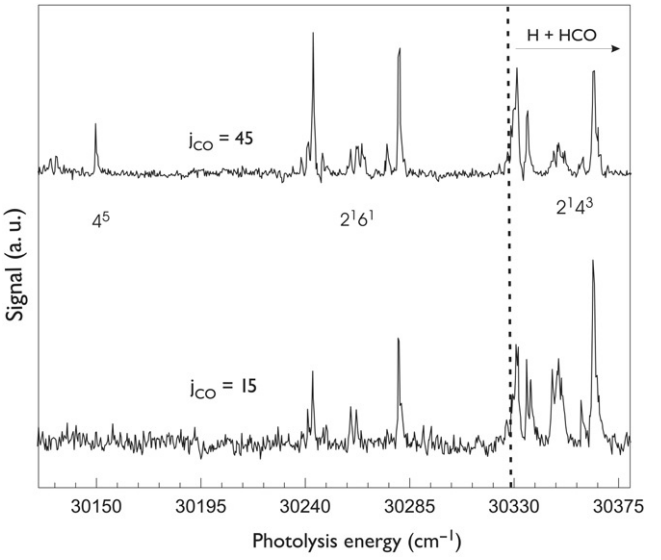

Figure 12. Phofex scan across the radical dissociation threshold (30 329 cm^{-1}) for indicated CO rotational levels.

one of the most fruitful systems with which to apply these methods. In probing the dynamics of the conventional molecular dissociation over the barrier, we used the detailed v_{H2}-j_{CO} correlation to model the exit channel dynamics in great detail. Perhaps more importantly, these state-correlated measurements have, in conjunction with the QCT calculations from the Bowman group, provided dramatic evidence of an important new roaming pathway in unimolecular dissociation. This has first allowed us to examine radical–radical reaction dynamics in new detail, using the roaming reaction as a sort of 'single-molecule reaction vessel'. We then used the energy dependence of the branching to roaming to explore the underlying dynamics of the roaming reaction itself, as well as to suggest the general importance of this phenomenon. We found roaming reactions to be directly related to the radical channel, in fact simply intramolecular abstraction reactions arising from frustrated radical dissociation events that occur within $\sim$100 cm^{-1} of the threshold for formation of a given product state of HCO.

The future prospects for these studies appear rich indeed. There are a number of open questions that remain to be addressed in the formaldehyde system alone. We have sketched our account of the energy-dependent branching but as yet we have not explored the details of possible 'mode specificity' in the multichannel branching. This could allow us to examine much more deeply those HCO states that will support roaming. We hope to use H_2 detection as a general probe of roaming. This will open up the investigations to many more systems beyond formaldehyde alone. Finally, Houston and Kable suggested that **v-J** correlation can be used to distinguish roaming from conventional molecular elimination, and Bowman and coworkers have recently confirmed this in QCT calculations for H_2CO [89]. This will represent another powerful tool in the effort to document this behaviour in other systems. At this point we

are confident that roaming behaviour is truly ubiquitous. To demonstrate this we need only develop our experimental eyes so we can see it.

Acknowledgements

We would like to thank Dave Townsend and Suk Young Lee for their contributions to the initial work. We thank Gregory E. Hall and Anatoly Komissarov for the finite slicing inversion program, as well as Wen Li for the IMACQ and IMAN programs. We acknowledge J. Bowman and his group (Emory University), and F. Suits (IBM) for their contributions. This work was supported by the Director, Office of Science, Office of Basic Energy Sciences, Division of Chemical Sciences, Geosciences and Biosciences, of the US Department of Energy and under the Contract Number: DE-FG02-04ER15593.

References

[1] B. A. DeGraff and J. G. Calvert, J. Am. Chem. Soc. **89**(10), 2247 (1967).
[2] J. G. Calvert, J. A. Kerr, K. L. Demerjian, and R. D. McQuigg, Science (Washington, DC, U. S.) **175** (4023), 751 (1972).
[3] P. L. Houston and C. B. Moore, J. Chem. Phys. **65**(2), 757 (1976).
[4] P. Ho, D. J. Bamford, R. J. Buss, Y. T. Lee, and C. B. Moore, J. Chem. Phys. **76**(7), 3630 (1982).
[5] P. Ho and A. V. Smith, Chem. Phys. Lett. **90**(6), 407 (1982).
[6] N. I. Sorokin, G. I. Skubnevskaya, and N. M. Bazhin, Teor. Eksp. Khim. **18**(4), 458 (1982).
[7] R. Koenig and J. Lademann, Chem. Phys. Lett. **94**(2), 152 (1983).
[8] D. J. Bamford, S. V. Filseth, M. F. Foltz, J. W. Hepburn, and C. B. Moore, J. Chem. Phys. **82**(7), 3032 (1985).
[9] T. J. Butenhoff, K. L. Carleton, and C. B. Moore, J. Chem. Phys. **92**(1), 377 (1990).
[10] T. J. Butenhoff, K. L. Carleton, R. D. Van Zee, and C. B. Moore, J. Chem. Phys. **94**(3), 1947 (1991).
[11] K. L. Carleton, T. J. Butenhoff, and C. B. Moore, J. Chem. Phys. **93**(6), 3907 (1990).
[12] D. Debarre, M. Lefebvre, M. Pealat, J. P. E. Taran, D. J. Bamford, and C. B. Moore, J. Chem. Phys. **83**(9), 4476 (1985).
[13] W. H. Green, Jr., C. B. Moore, and W. F. Polik, Annu. Rev. Phys. Chem. **43**, 591 (1992).
[14] C. B. Moore and J. C. Weisshaar, Annu. Rev. Phys. Chem. **34**, 525 (1983).
[15] R. D. van Zee, M. F. Foltz, and C. B. Moore, J. Chem. Phys. **99**(3), 1664 (1993).
[16] A. C. Terentis and S. H. Kable, Chem. Phys. Lett. **258**(5,6), 626 (1996).
[17] M. J. Dulligan, M. F. Tuchler, J. Zhang, A. Kolessov, and C. Wittig, Chem. Phys. Lett. **276**(84), 84 (1997).
[18] A. C. Terentis, S. E. Waugh, G. F. Metha, and S. H. Kable, J. Chem. Phys. **108**(8), 3187 (1998).
[19] L. R. Valachovic, M. F. Tuchler, M. Dulligan, T. Droz-Georget, M. Zyrianov, A. Kolessov, H. Reisler, and C. Wittig, J. Chem. Phys. **112**(6), 2752 (2000).
[20] H. -M. Yin, K. Nauta, and S. H. Kable, J. Chem. Phys. **122**(19), 194312/1 (2005).
[21] H. M. Yin, S. H. Kable, X. Zhang, and J. M. Bowman, Science **311**, 1443 (2006).
[22] M. Tulej, G. Knopp, P. Beaud, T. Gerber, and P. P. Radi, J. Raman Spectrosc. **36**(2), 109 (2005).
[23] M. J. Frisch, R. Krishnan, and J. A. Pople, J. Phys. Chem. **85**(11), 1467 (1981).
[24] J. A. Pople and J. W. Sidman, J. Chem. Phys. **27**, 1270 (1957).
[25] J. D. Goddard and H. F. Schaefer, J. Chem. Phys. **70**(11), 5117 (1979).
[26] V. Bachler and E. A. Halevi, Theor. Chim. Acta **59**(6), 595 (1981).
[27] J. D. Goddard, Y. Yamaguchi, and and H. F. Schaefer, III, J. Chem. Phys. **75**(7), 3459 (1981).
[28] S. K. Gray, W. H. Miller, Y. Yamaguchi, H. F. Schaefer, and III, J. Am. Chem. Soc. **103**(8), 1900 (1981).
[29] M. Dupuis, W. A. Lester, Jr., B. H. Lengsfield, III, and B. Liu, J. Chem. Phys. **79**(12), 6167 (1983).
[30] K. Johst and H. Johansen, Zeitschrift fuer Physikalische Chemie (Leipzig) 266 (1), 17 (1985).
[31] Y. T. Chang, C. Minichino, and W. H. Miller, J. Chem. Phys. **96**(6), 4341 (1992).
[32] D. Feller, M. Dupuis, and B. C. Garrett, J. Chem. Phys. **113**(1), 218 (2000).
[33] L. M. M. de Martins, G. Arbilla, and E. C. da Silva, J. Phys. Chem. A **102**(52), 10805 (1998).
[34] W. Chen, W. L. Hase, and H. B. Schlegel, Chem. Phys. Lett. **228**(4–5), 436 (1994).

[35] X. Li, J. M. Millam, and H. B. Schlegel, J. Chem. Phys. **113**(22), 10062 (2000).
[36] R. Schinke, J. Chem. Phys. **84**(3), 1487 (1986).
[37] X. Zhang, S. Zou, L. B. Harding, and J. M. Bowman, J. Phys. Chem. A **108**(41), 8980 (2004).
[38] X. Zhang, J. L. Rheinecker, and J. M. Bowman, J. Chem. Phys. **122**(11), 114313 (2005).
[39] X. Zhang and J. M. Bowman, Phys. Chem. Chem. Phys. **8**, 321 (2006).
[40] J. L. Rheinecker, X. Zhang, and J. M. Bowman, Mol. Phys. **103**(6–8), 1067 (2005).
[41] C. R. Gebhardt, T. P. Rakitzis, P. C. Samartzis, V. Ladopoulos, and T. N. Kitsopoulos, Rev. Sci. Instrum. **72**(10), 3848 (2001).
[42] D. Townsend, M. P. Minitti, and A. G. Suits, Rev. Sci. Instrum. **74**(4), 2530 (2003).
[43] J. J. Lin, J. G. Zhou, W. C. Shiu, and K. P. Liu, Rev. Sci. Instrum. **74**(4), 2495 (2003).
[44] D. Townsend, S. A. Lahankar, S. K. Lee, S. D. Chambreau, A. G. Suits, X. Zhang, J. Rheinecker, L. B. Harding, and J. M. Bowman, Science (Washington, DC, U. S.) 306 (5699), 1158 (2004).
[45] S. D. Chambreau, S. A. Lahankar, and A. G. Suits, J. Chem. Phys. **125**(4), 044302 (2006).
[46] S. A. Lahankar, S. D. Chambreau, D. Townsend, F. Suits, J. Farnum, X. Zhang, J. M. Bowman, and A. G. Suits, J. Chem. Phys. **125**(4), 044303 (2006).
[47] S. A. Lahankar, S. D. Chambreau, X. Zhang, J. M. Bowman, and A. G. Suits, J. Chem. Phys. **126**(4), (2007).
[48] B. Schramm, D. J. Bamford, and C. B. Moore, Chem. Phys. Lett. **98**(4), 305 (1983).
[49] Y. Yamaguchi, S. S. Wesolowski, T. J. van Huis, and H. F. Schaefer III, J. Chem. Phys. **108**, 5281 (1998).
[50] L. J. Butler and D. M. Neumark, J. Phys. Chem. **100**(31), 12801 (1996).
[51] G. E. Hall, N. Sivakumar, P. L. Houston, and I. Burak, Phys. Rev. Lett. **56**(16), 1671 (1986).
[52] G. E. Hall, N. Sivakumar, D. Chawla, P. L. Houston, and I. Burak, J. Chem. Phys. **88**(6), 3682 (1988).
[53] G. E. Hall and P. L. Houston, Annu. Rev. Phys. Chem. **40,** 375 (1989).
[54] A. S. Bracker, E. R. Wouters, A. G. Suits, and O. S. Vasyutinskii, J. Chem. Phys. **110**(14), 6749 (1999).
[55] M. Wu and G. E. Hall, Journal of Photochemistry and Photobioloyg a chemistry A **80**(1–3), 45 (1994).
[56] S. W. North and G. E. Hall, J. Chem. Phys. **106**(1), 60 (1997).
[57] G. E. Hall, A. V. Komissarov, and T. J. Sears, J. Phys. Chem. A **108**(39), 7922 (2004).
[58] A. P. Clark, M. Brouard, F. Quadrini, and C. Vallance, Phys. Chem. Chem. Phys. **8**(48), 5591 (2006).
[59] A. G. Suits, and O. S. Vasyutinskii, Chem. Rev. (in press).
[60] A. Ticktin and J. R. Huber, Chem. Phys. Lett. **156**(4), 372 (1989).
[61] K. H. Gericke, H. G. Glaser, C. Maul, and F. J. Comes, J. Chem. Phys. **92**(1), 411 (1990).
[62] W. Li, S. D. Chambreau, S. A. Lahankar, and A. G. Suits, Rev. Sci. Instrum. **76**(6), 063106/1 (2005).
[63] D. Townsend, W. Li, S. K. Lee, R. L. Gross, and A. G. Suits, J. Phys. Chem. A **109**(39), 8661 (2005).
[64] M. Brouard, M. T. Martinez, and J. Omahony, Mol. Phys. **71**(5), 1021 (1990).
[65] M. Drabbels, C. G. Morgan, D. S. McGuire, and A. M. Wodtke, J. Chem. Phys. **102**(1), 611 (1995).
[66] C. G. Morgan, M. Drabbels, and A. M. Wodtke, J. Chem. Phys. **105**(11), 4550 (1996).
[67] M. L. Costen, H. Katayanagi, and G. E. Hall, J. Phys. Chem. A **104**(45), 10247 (2000).
[68] A. V. Komissarov, M. P. Minitti, A. G. Suits, and G. E. Hall, J. Chem. Phys. **124**(1), 14303 (2006).
[69] J. J. Lin, J. G. Zhou, W. C. Shiu, and K. P. Liu, Science **300**(5621), 966 (2003).
[70] J. G. Zhou, J. J. Lin, and K. P. Liu, J. Chem. Phys. **119**(16), 8289 (2003).
[71] J. G. Zhou, J. Lin, W. C. Shiu, and K. P. Liu, J. Chem. Phys. **119**(10), 4997 (2003).
[72] A. T. J. B. Eppink and D. H. Parker, Rev. Sci. Instrum. **68**(9), 3477 (1997).
[73] D. W. Chandler and P. L. Houston, Journal of Physics chemistry Chem. **87**, 1445 (1987).
[74] C. Zauli, Journal of Physics chemistry **79**(3), 555 (1994).
[75] R. H. Judge and D. J. Clouthier, Comput. Phys. Commun. **135**(3), 293 (2001).
[76] G. W. T. M. J. Frisch, H. B. Schlegel, G. E. Scuseria, M. A. Robb, J. R. Cheeseman, J. A. Montgomery, Jr., T. Vreven, K. N. Kudin, J. C. Burant, J. M. Millam, S. S. Iyengar, J. Tomasi, V. Barone, B. Mennucci, M. Cossi, G. Scalmani, N. Rega, G. A. Petersson, H. Nakatsuji, M. Hada, M. Ehara, K. Toyota, R. Fukuda, J. Hasegawa, M. Ishida, T. Nakajima, Y. Honda, O. Kitao, H. Nakai, M. Klene, X. Li, J. E. Knox, H. P. Hratchian, J. B. Cross, V. Bakken, C. Adamo, J. Jaramillo, R. Gomperts, R. E. Stratmann, O. Yazyev, A. J. Austin, R. Cammi, C. Pomelli, J. W. Ochterski, P. Y. Ayala, K. Morokuma, G. A. Voth, P. Salvador, J. J. Dannenberg, V. G. Zakrzewski, S. Dapprich, A. D. Daniels, M. C. Strain, O. Farkas, D. K. Malick, A. D. Rabuck, K. Raghavachari, J. B. Foresman, J. V. Ortiz, Q. Cui, A. G. Baboul, S. Clifford, J. Cioslowski, B. B. Stefanov, G. Liu, A. Liashenko, P. Piskorz, I. Komaromi, R. L. Martin, D. J. Fox, T. Keith, M. A. Al-Laham, C. Y. Peng, A. Nanayakkara, M. Challacombe, P. M. W. Gill, B. Johnson, W. Chen, M. W. Wong, C. Gonzalez, and J. A. Pople, Gaussian 03 (Wallingford CT, 2004, 2003).
[77] H. Eyring, J. Chem. Phys. **3** 107 (1935).
[78] H. Eyring, Chem. Rev. **17** 65 (1935).
[79] J. I. Steinfeld, J. S. Francisco, and W. L. Hase, *Chemical Kinetics Dynamics, Second Edition*. Prentice-Hall (1999).

[80] T. P. Marcy, R. R. Diaz, D. Heard, S. R. Leone, L. B. Harding, and S. J. Klippenstein, J. Phys. Chem. **105**, 8361 (2001).
[81] T. Y. Yan, C. Doubleday, and W. L. Hase, J. Phys. Chem. A **108**, 9863 (2004).
[82] F. Mohammad, V. R. Morris, W. H. Fink, and W. M. Jackson, J. Phys. Chem. **97**(45), 11590 (1993).
[83] P. L. Houston, and S. H. Kable, *Proceedings of the National Academy of Sciences* (2006).
[84] L. Rubio-Lago, G. A. Amaral, A. Arregui, J. G. Izquierdo, F. Wang, D. Zaouris, T. N. Kitsopoulos, and L. Banares, Phys. Chem. Chem. Phys. (submitted) (2007).
[85] A. E. Pomerantz, J. P. Camden, A. S. Chiou, F. Ausfelder, N. Chawla, W. L. Hase, and R. N. Zare, J. Am. Chem. Soc. **127**, 16368 (2005).
[86] J. Troe, J. Phys. Chem. **88**(19), 4375 (1984).
[87] J. Troe, J. Phys. Chem. A **109**, 8320 (2005).
[88] J. Troe, J. Phys. Chem. A **111**(19), 3862 (2007).
[89] J. D. Farnum, X. B. Zhang, and J. M. Bowman, J. Chem. Phys. **126**(13) (2007).